

RespEnh: A Technique for Enhancing Respiration Sensing in Interference Scenarios With Wi-Fi Signal

Jingjing Fan^{ID}, Chenyu Pan^{ID}, Guanhua Zhao^{ID}, Xinyu Tong^{ID}, Keqiu Li^{ID}, *Fellow, IEEE*, and Shisheng Huang

Abstract—Wi-Fi-based noncontact respiratory monitoring technology plays a significant role in smart elderly care by eliminating the need for users to wear additional hardware devices. Although respiration sensing has shown impressive accuracy in ideal scenarios, achieving precise respiration monitoring in interfering scenarios, such as when other users, are engaged in activities, remains challenging. This difficulty arises primarily from the weak nature of the respiratory signal, which is susceptible to interference from activities. To address this issue, this article introduces the *RespEnh* system, a respiratory monitoring system that utilizes human location information to mitigate interference. First, We enhance the quality of respiratory signal by leveraging the frequency diversity of Wi-Fi signal, effectively visualizing respiratory patterns even amidst interference. Second, we apply short time window shift to remove walking noise in the time domain while preserving respiratory signal characteristics. Finally, we integrate multiantenna signals to enhance spatial domain performance. Experimental results demonstrate that our system achieves a relative anti-interference performance of 2.4 m, even when breathing as far away as 6.4 m. It effectively monitors person's respiration, with a detection rate of 80% within an error range of 1 bpm.

Index Terms—Channel state information (CSI), interference, respiration sensing, Wi-Fi sensing.

I. INTRODUCTION

RESPIRATION is an important indicator of disease progression and health decline according to medical research, and it consists of two main indicators: 1) respiration rate and 2) respiration pattern. Early respiration monitoring usually requires contact measurements by wearing pressure sensors or wearable devices, which easily cause discomfort for special populations, such as the elderly, and the wearable method greatly limits its application. In recent years, noncontact measurement methods based on radar signals [1], [2], [3], [4], [5], [6], radio-frequency signals (e.g., RFID [7], [8], [9], Wi-Fi [10], [11], [12], [13], [14], [15], [16], [17], [18], LoRa [19], [20], [21], etc.), and acoustic signals [22], [23], [24]

Manuscript received 26 March 2024; revised 17 May 2024; accepted 30 May 2024. Date of publication 10 June 2024; date of current version 7 November 2024. This work was supported by the National Natural Science Foundation of China under Grant 62102282 and Grant 62372324.

(Corresponding author: Xinyu Tong.)

Jingjing Fan, Chenyu Pan, Guanhua Zhao, Xinyu Tong, and Keqiu Li are with the College of Intelligence and Computing, Tianjin University, Tianjin 300350, China (e-mail: jingjingfan@tju.edu.cn; panchenyu@tju.edu.cn; zhaogh@tju.edu.cn; xytong@tju.edu.cn; keqiu@tju.edu.cn).

Shisheng Huang is with Yangtze River Delta Anneng New Energy Technology (Shanghai) Company Ltd., Shanghai 200335, China (e-mail: huangshisheng@yrdne.com).

Digital Object Identifier 10.1109/JIOT.2024.3411605

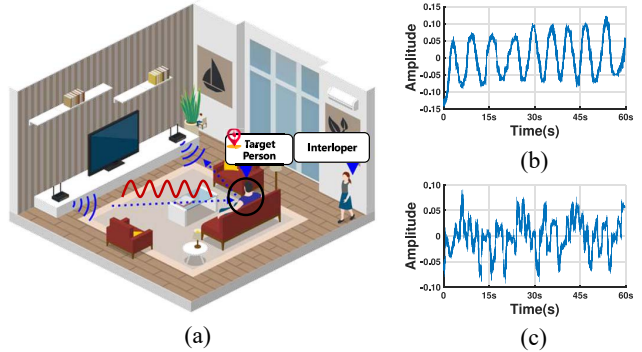


Fig. 1. Comparison of respiratory waveforms for the interference scenario and the noninterference scenario. (a) Represents the respiration perception scene with interference. (b) and (c) Represent the monitored respiratory waveforms in the noninterference and interference scenarios, respectively, where the ground truth for each are 10 and 16 bpm, respectively.

have attracted extensive attention from researchers at home and abroad. Among them, Wi-Fi signals provide great convenience for respiratory sensing due to the advantages of high popularity, low cost, and small bandwidth, so Wi-Fi sensing has become an effective means to conduct respiratory monitoring.

Existing works of Wi-Fi respiratory monitoring are mainly achieved by deploying a set of commercial Wi-Fi devices in free space to monitor human respiratory behavior. The periodic contraction or expansion of the chest cavity due to respiration will cause periodic changes in the length of Wi-Fi reflected signal path. This small chest displacement makes the work of respiration monitoring challenging. Existing works have established corresponding theoretical models toward pure respiration scenarios, but suffer from large waveform distortions and low-monitoring accuracy when there are other interferences or large noises in the surroundings, as shown in Fig. 1. Therefore, how to effectively enhance the respiration signal and suppress interference to achieve respiration sensing under interference scenarios becomes an important challenge in the present work.

To solve the interference problem, some scholars have researched on it, and the existing methods are roughly divided into two categories.

- 1) Special deployment of transceivers to narrow the perception range. Zeng et al. [25] point out that the placement of transceivers will have a noticeable impact on the perception range and boundaries, which indicates that interference can be excluded from the perception through the reasonable placement of transceivers. However, this method requires a high-deployment

environment, and once deployed, it can only sense targets within a limited sensing range, with poor flexibility and restricted sensing area. For example, it usually needs to extend the transmitter-receiver distance to 10 m to avoid interference within the effective sensing range at home, which makes it difficult to deploy flexibly.

- 2) Obtaining highly accurate Time of Flight (ToF) and Angle of Arrival (AoA) for localization of human breath and interference. Xie [46] and Zhang [45] proposed the use of large-scale antenna arrays can obtain accurate ToF and AoA for localization of the human body and interferer, respectively. However, this method requires strict antenna phase calibration on commercial Wi-Fi devices. Even after calibration, some position estimation bias still occurs after parameter acquisition. Therefore, we need to explore a robust anti-jamming system that is deployment-independent and does not require large-scale antenna arrays.

In this article, we propose *RespEnh*, a robust respiratory sensing system based on commercial Wi-Fi devices, which eliminates the need for phase calibration and enables accurate respiratory monitoring over a range of interference distances based on a pair of fixed transceiver, is simple and inexpensive to deploy. While in actual deployment, the following main challenges are faced, for which we propose corresponding solutions:

Challenge 1—How to Better Separate the Walking Signal and the Breathing Signal? To achieve accurate respiration detection in interference scenarios, an intuitive idea is to separate the interfering signal directly. However, we found that the walking signal is irregularly closely related to the trajectory, which cannot be cleanly and completely separated when it overlaps with the breathing signal. To address this problem, we use the method of enhancing breathing and suppressing walking signal to indirectly approximate the interfered signal to pure breathing signal. This is because we find that although the walking signal is irregular, its rapidly changing characteristics can be distinguished from the slowly changing breathing signal, this difference inspires us to use the short time window shift method.

Challenge 2—How to Fully Incorporate Frequency Domain Information to Achieve Maximum Signal Gain? Due to the frequency diversity technique adopted by commercial Wi-Fi devices, the signal is transmitted by multiple subcarriers at the same time. Combined with the spatial projection mechanism, each subcarrier corresponds to an optimal waveform and projection angle, all projection angles can be fitted to a straight line whose slope reflects the ToF. This method is extremely different from the traditional model used for ToF parameter estimation, so we establish a linear projection mechanism specific to respiratory signal. At the same time, we use this mechanism to achieve fixed-point qualitative enhancement of human respiratory signal to achieve the purpose of enhancing the proportion of respiratory signal in the mixed signal.

Challenge 3—How to Fully Combine the Airspace Information to Get the Maximum Monitoring Accuracy? Existing works tend to use only a single antenna ratio or directly combine all antenna ratios in space to estimate the

result, but in scenarios with interference, the quality of antenna channel state information (CSI) still varies greatly even after preprocessing due to the different spatial locations. In this regard, we urgently need a metric to measure the good or bad quality of antennas. Combining the analysis of broad data and the periodic characteristic of respiration, we propose a new metric -peak-to-average ratio (PAR) * breath signal-to-noise ratio (BNR) to achieve antenna quality screening, combined with the use of one or more antennas of better quality to estimate the respiration rate.

To address the above challenges, we design the *RespEnh* system, a respiratory enhancement system based on commercial Wi-Fi devices that enables robust respiratory monitoring in disturbed scenarios. The contributions of this article are mainly in the following three aspects.

- 1) For the first time, we use the linear projection rule satisfied by Wi-Fi signal to achieve the enhancement of breathing signal in mixed signal with interference, which enables the weak breathing signal to have an increased component and completes a one-time enhancement of the breathing signal.
- 2) We observe a significant difference in the characteristics of walking and breathing signals. The walking signal exhibits rapid changes, whereas the breathing signal varies more gradually. To address this, we employ short-window strong filtering to splice multiple data segments, ensuring that the characteristics of the breathing signal are maximized while effectively suppressing the walking signal components.
- 3) We carry out extensive experiments in two scenarios by controlling variables to demonstrate the anti-jamming perception boundaries of the proposed system. The experimental results show that, compared with the existing systems, the proposed method can achieve effective perception of breathing at 6.4 m under 2.4-m anti-jamming conditions, and the perception accuracy reaches 80%.

The remainder of this article is organized as follows. Related work is presented in Section II, and the preliminary is introduced in Section III. The system framework and design details are provided in Sections IV and V individually. Section VI describes the relevant experimental setup as well as the results, according to which we evaluated the system. Then Section VII contains a discussion, including future improvement methods and other feasible work. Finally, this article is summarized in Section VIII.

II. RELATED WORK

Traditional respiration detection commonly employs wearable devices [26], [27] pressure sensors [28], [29] and watch bands for direct measurement. However, these contact-based measurements may present challenges in applicability, especially for specific groups, such as the elderly. On the contrary, noncontact measurement offers several advantages. Presently, the mainstream measurement methods can be broadly classified into two categories: 1) radar-based respiration measurement and 2) Wi-Fi-based respiration measurement.

A. Radar-Based Respiration Measurement

Radar-based measurements include the use of CW Doppler radar [1], [2], UWB radar [3], [4], [5], FMCW radar [6], and solutions using universal software radio peripheral (USRP) [12] for human respiration rate estimation. CW Doppler radar-based methods have low-power consumption and simple structure but are susceptible to ambient noise and multipath effects. UWB radars have large bandwidth requirements (1 and 2 GHz) and high-pulse width and peak signal strength requirements, which increase hardware requirements and system complexity. FMCW radars require even higher bandwidths on the hardware side (1.79 GHz), which are costly and not very practical.

B. Wi-Fi-Based Respiration Measurement

1) *RSS-Based Measurement*: Ordinary commercial Wi-Fi hardware devices have a bandwidth of 20/40 MHz, which is much lower than the bandwidth requirements of UWB radar and FMCW radar systems, greatly reduces the deployment requirements, and thus has become the focus of many researchers and scholars' studies. The received signal strength (RSS) signals [10], [30], [31], [33] can reflect the changes in human respiration, but they are not very sensitive, and the measurement range is restricted and required to be near the LOS. UbiBreathe [10] demonstrates that Wi-Fi RSS is affected by the respiratory process, and thus RSS data streams can be used to extract respiratory information. Literature [32] uses the proposed RSS model for respiration rate estimation. However, in practice, the use of RSS is only feasible when the subject is located near the LOS, and since the changes in RSS caused by exhalation and inhalation are very small and can be easily drowned out by ambient noise, the use of RSS data streams does not allow sensitive tracking of small movements in the chest due to breathing [34], which is even less advantageous for the measurement of respiration rate in dynamic environments. Therefore, researchers have shifted their goal to CSI data, which is richer in information and more sensitive to respiration, to extract respiratory information [35].

2) *CSI-Based Measurement*: CSI contains both amplitude and phase information. Studies have shown that CSI amplitude has obvious mathematical and physical relationships with human activity [36], so CSI amplitude can be used to reflect the respiration rate, but literature [34] shows that there is a “blind spot problem” when using CSI amplitude information alone, and then it is proposed and combined with the Fresnel model [34] to explain the reason for the “blind spot problem.” Based on the Fresnel diffraction model, Zhang et al. [37] accurately quantified the relationship between the diffraction gain and the subtle displacement of the chest of the human target for the first time, and successfully transforms the previously considered “destructive” diffraction hindrance of the first Fresnel zone (FFZ) into a beneficial perceptual capability. The actual received CSI phase information is much noisy and usually suffers from sample frequency offsets (SFOs), carrier frequency offsets (CFOs), and packet detection delays (PDDs) [38] and is not directly usable, and although some methods have been used to correct for the phase offsets [39], [40], [41], they still do not allow for good detection of

millimeter-scale fine-grained chest displacements, the results are not very satisfactory. Fullbreathe [42] points out that CSI's amplitude and phase are perfectly complementary, and the combination of the two can eliminate blind spots and extends the range of perception. In this regard, Farsense [38] proposes improving detection by combining the real and imaginary parts of the CSI ratio, which extends the sensing range from 3 and 4 to 8 and 9 m. However, it mainly focuses on pure breathing scenarios, when faced with interference, the system can easily fail.

C. Comparison With State-of-the-Art

Recent work has shown that the metric that affects the received signal quality of a sensing system is the sensing signal-noise ratio (SSNR) [25], [43]. The higher the SSNR value is, the higher the quality of the sensed signals are, and by increasing the SSNR metrics the sensing distance can be improved and the sensing boundary can be expanded. Methods to improve SSNR include combining the use of multiple antennas and multiple subcarriers [25], [43], [44].

The interference problem is unavoidable when the sensing system is deployed in practice, and most of the existing works [25], [38], [44] focus on how to continuously improve the sensing range and boundaries, ignoring the solution of the interference problem, and due to the weak nature of the respiratory signal, the performance of the system drops linearly when the interference is introduced into the system, and lacks an effective separation method for separating the interference from the target signals, and the idea of placing the transceiver in EMA [25] becomes an important reference to solve the interference of the breathing system, but there is no effective work to solve the anti-interference problem in the case of fixed transceivers, at the same time, this method has high requirements for the deployment of the environment and restricted perception range, once the deployment is determined, it can only be perceived for the targets within the limited perception range, with poor flexibility and restricted perception area.

In summary, this article discusses the interference problem, and the designed *RespEnh* system becomes the first work to realize the respiratory perception in the interference scene.

III. BASIC IDEA

In this section, we first introduce the fundamental principle of breath sensing in Wi-Fi free space by combining Fresnel model with CSI model. Then we illustrate how human motion changes the Wi-Fi signal, comparing the variability with breathing in terms of physical space and signal overlay dimensions, respectively. Finally, we address the challenges facing this system from the perspective of both the significant differences between walking and breathing signal and the unique linear projection rule for breathing signal.

A. Respiration Sensing Using CSI

The effects of reflection, refraction and diffraction that Wi-Fi propagates from the transmitter to the receiver can be characterized by CSI, which is a fine-grained state information that describes the propagation characteristics of a wireless channel through the channel frequency response (CFR) of

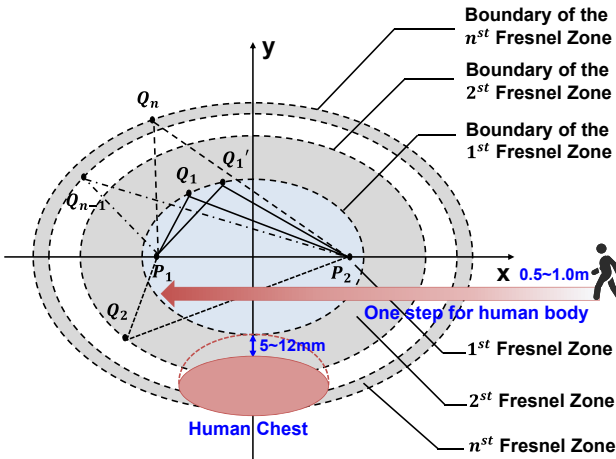


Fig. 2. Schematic of the Fresnel zone.

each subcarrier, reflecting the changing characteristics of the surrounding environment. Due to the multipath effect, the signal received at the receiver is often a superposition of signals from multiple paths. Therefore, the CSI at moment t can be expressed as

$$H(f, t) = \sum_{l=1}^N a_l(f, t) e^{-j2\pi f \frac{d_l(t)}{c}} \quad (1)$$

where N denotes the number of indoor propagation paths, f denotes the frequency of the subcarrier, c is the speed of light, $a_l(f, t)$ denotes the complex number of amplitude decays, and the initial phases for the l th path, this complex coefficient is mainly determined by the length of the reflection path (RPL) and the size and material of the reflecting surface, $d_l(t)$ denotes the reflected path length of the l th path.

In the physical spatial dimension, CSI manifests itself as a cut in the Fresnel zone by motion. As shown in Fig. 2, the thoracic displacement produced by respiration is about $5 \sim 12$ mm, which is much smaller than the Wi-Fi wavelength of 5.24 GHz (5.7 cm), and thus behaves as an approximate constant in amplitude, and as a rotation of an angle of $\pi/3 \sim 2\pi/3$ in phase, i.e., it behaves as a small arc of a circle in the complex plane, as shown in Fig. 3, where P_1 and P_2 denote the starting points of inhalation and respiration, respectively. The circular arc in the middle reflects the CSI due to respiration.

In the signal superposition dimension, as shown in Fig. 3, CSI can be represented as a superposition of multiple path signals. These propagation paths can be generally divided into two groups: 1) static paths and 2) dynamic paths. Static paths represent the direct path signals from the transmitter to the receiver and the surrounding signals reflected from stationary objects (e.g., walls, floors, etc.). Dynamic paths include paths of signal changes reflected by human movement (e.g., breathing) in the absence of interference. When only breathing is present in the environment, the received CSI signal can be expressed as the following equation:

$$\begin{aligned} H(f, t) &= H_s(f, t) + H_d(f, t) + \varepsilon(f, t) \\ &= \sum_{i \in \Omega_s} H_i(f, t) + \sum_{j \in \Omega_d} H_j(f, t) + \varepsilon(f, t) \end{aligned} \quad (2)$$

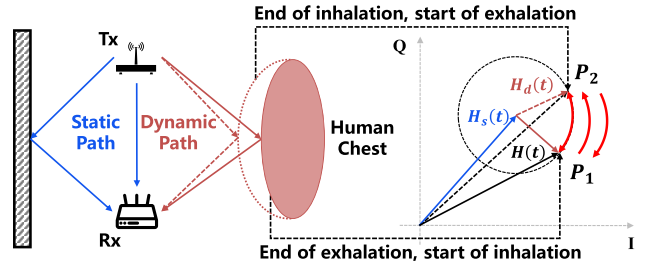


Fig. 3. Schematic of respiration sensing.

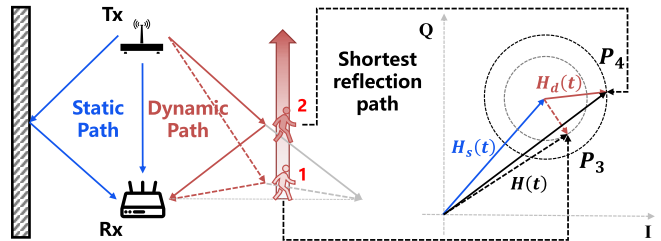


Fig. 4. Schematic of walk sensing.

where Ω_s denotes the set of static paths, Ω_t denotes the set of dynamic paths, $H_i(f, t)$ indicates the signal of the i th static path, $H_j(f, t)$ indicates the signal of the j th dynamic path, and $\varepsilon(f, t)$ is the thermal noise.

B. Motion Sensing Using CSI

External movement behavior also causes a change in the reflected path length, which can also be sensed by Wi-Fi. When there is interference in the environment, the CSI manifestation changes accordingly. Since the walking CSI signal is closely related to the trajectory, only a small section of the extraction here trajectory as an analysis.

In the physical space dimension, since one step of the human body when walking is about $0.5 \sim 1.0$ m, which is much larger than the Wi-Fi wavelength, one step will cross multiple Fresnel bands. The walking signal can be manifested as a fluctuating change in CSI amplitude related to the walking trajectory, and as a sequential inclusion of multiple cycles in phase. As shown in Fig. 4, when the human body walks from Position 1 to Position 2, it is the process of moving from P_3 to P_4 in a spiral rotational movement, accompanied by a gradual increase in amplitude and multiple cycles in phase changes, the walking process is much more complex compared to breathing.

In the signal superposition dimension, it is the same as the respiratory CSI, which still includes two groups of path signals: 1) static paths and 2) dynamic paths. However, in a pure breathing scenario, there is only one dynamic RPL, whereas in a scenario with interference, the dynamic RPL consists of two paths: 1) a change in the RPL due to the target character's breathing and 2) a change in the RPL introduced by the interferer's walking, so the CSI signal at this moment can be expressed as

$$\begin{aligned} H(f, t) &= H_s(f, t) + H_d(f, t) + \varepsilon(f, t) \\ &= \sum_{i \in \Omega_s} H_i(f, t) + \sum_{j_1 \in \Omega_{d1}} H_{j_1}(f, t) \\ &\quad + \sum_{j_2 \in \Omega_{d2}} H_{j_2}(f, t) + \varepsilon(f, t) \end{aligned} \quad (3)$$

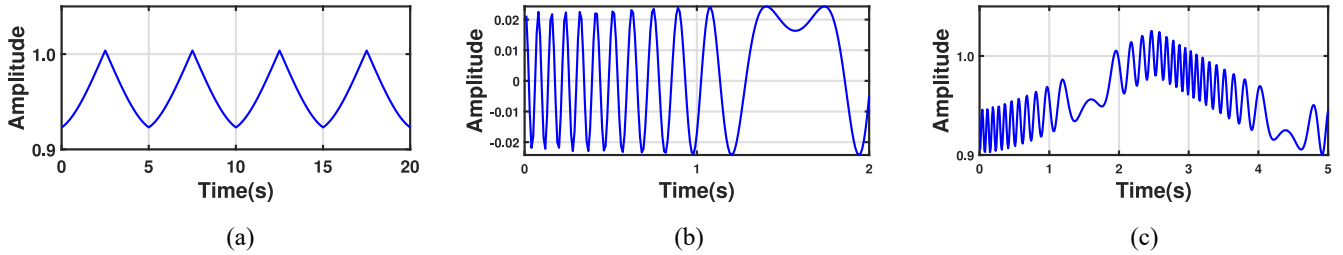


Fig. 5. Differences of breath, walk, and mixed signal. (a) Breath signal. (b) Walk signal. (c) Mixed signal.

where Ω_s denotes the set of static paths, $H_s(f, t)$ and $H_d(f, t)$ denote the static and dynamic reflected signals, the $\varepsilon(f, t)$ is the thermal noise, and Ω_{d1} and Ω_{d2} denote the set of dynamic paths of respiration and walking, respectively.

In this case, for the presence of interference, the dynamic CSI signal received at the receiver can be specifically represented as

$$H_d(f, t) = a_t(f, t)e^{-j2\pi f \frac{d_t(t)}{c}} + a_i(f, t)e^{-j2\pi f \frac{d_i(t)}{c}} \quad (4)$$

where $H_d(f, t)$ represents the sum of dynamic signals in the environment, $a_t(f, t)$ and $2\pi f(d_t(t)/c)$ denotes the complex coefficient and phase delay introduced by respiration of the target person, and $a_i(f, t)$ and $2\pi f(d_i(t)/c)$ denotes the complex coefficient and phase delay introduced by the motion of the interferer.

C. Differences in Motion and Respiration Signal

According to the above characteristics, we combine the features and advantages of the pure breath sensing algorithm with the specificity of the interference scene, starting from two aspects: 1) walking is not consistent with the speed of change of the respiratory signal and 2) the optimal projection axis of the respiratory signal satisfies the law of linear change.

The walking and breathing signals are significantly different, mainly in the inconsistency of their speed of change. The breathing signal tends to have a period of a few seconds and changes slowly, as shown in the Fig. 5(a), and the corresponding dynamic component of the signal in the complex plane can be regarded as a vector with constant amplitude and varying phase between $\pi/3$ and $2\pi/3$. In contrast, the walking signal changes more rapidly. First, the amplitude changes quickly, crossing multiple Fresnel bands per second, and the amplitude of the corresponding dynamic component of the signal cannot be regarded as unchanged. Second, the phase, as the displacement generated by the human body's walking is much larger than the wavelength of the Wi-Fi (5.7 cm) per second, the phase of the walking signal changes even more dramatically, often rotating multiple times around the complex plane in one second, as shown in Fig. 5(b). When the breath signal is mixed with the walking signal, the received CSI signal shows the pattern of change as shown in Fig. 5(c). It is similar to the continuous wave with breathing signal amplitude modulation and walking signal frequency modulation, and this characteristic makes it more effective to filter out the breathing

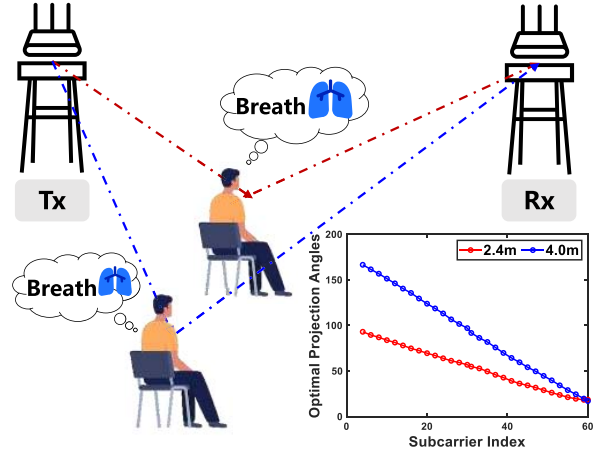


Fig. 6. Best projection degrees of different distances.

signal with walking interference by using the short window strong filter.

D. Linear Projection Rules for Respiration CSI

The optimal projection axis of the breathing signal satisfies the linear change law. In the pure breathing scenario, we find that the optimal projection axis between multiple subcarriers at the same distance satisfies the linear variation rule, as shown in

$$\Delta\theta = -2\pi \Delta f \frac{\Delta d(t)}{c} \quad (5)$$

where $\Delta d(t)$ denotes the difference between the length of the reflected path and the direct path, Δf denotes the frequency interval between neighboring subcarriers, c denotes the speed of light, and $\Delta\theta$ reflects the slope of the best projection curve. When $\Delta d(t)$ is different, the slopes of the corresponding curves are also different. As shown in Fig. 6, the two fitted straight lines in the figure represent the optimal projection angles of the respiratory signals received at each subcarrier when the human body is located at 2.4 and 4.0 m, respectively, and the one with a large slope is the scenario of respiration at 4.0 m.

In an environment with only one target person, the dynamic path originates only from the Wi-Fi reflection changes caused by the chest changes corresponding to human breathing, while in a scene with interference, the dynamic path contains two: 1) the dynamic path with small amplitude periodic changes caused by human breathing and 2) the dynamic path with fast

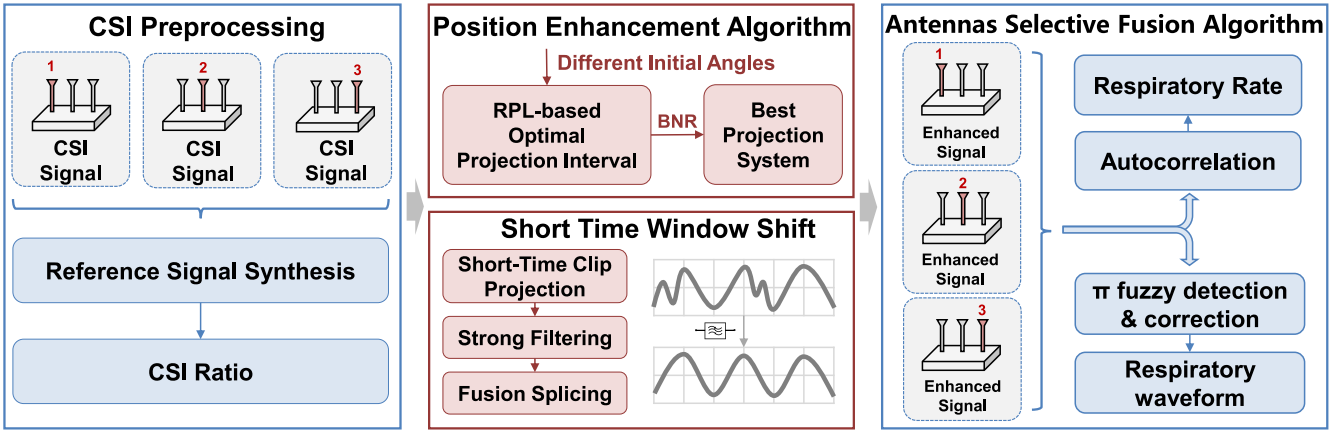


Fig. 7. *RespEnh* system overview.

and irregular changes caused by interfering people walking. To address this feature in the walking scene, we design a breath perception algorithm enhanced by distance, which makes it possible to calculate the optimal projection interval according to the reflected path length at a known location when the optimal projection axis cannot be accurately found due to the interference of the walking signal, and combine it with the initial angle traversal mechanism to search for the best matching set of optimal projection angles under the current data, to achieve the maximization of the breathing feature of the mixed signal and realize the purpose of enhancing the breathing signal.

IV. SYSTEM FRAMEWORK

RespEnh system is a noncontact anti-jamming respiratory sensing system for commercial Wi-Fi devices, which aims at accurately detecting and directionally enhancing the respiratory signals of target human under interference scenarios, eventually to improve the existing respiratory systems that suffer from large detection errors and serious waveform distortions in such scenarios. The overview of *RespEnh* system, which is shown in Fig. 7, consists of the following four parts:

Data Preprocessing: To obtain CSI signals without random phase noise, such as CFO, SFO, PDD, etc., and to prevent direct antenna ratio from destroying the respiratory signal characteristics, we need to implement this operation first. This part mainly consists of two elements: 1) equivalent signal analysis and 2) reference CSI ratio. First, the reference signal is obtained by equivalent signal analysis, i.e., appropriate weights are selected to make full use of the signals from the three antennas to obtain a synthesized signal with minimal dynamic fluctuations. Second, we use the CSI Ratio model to obtain the preprocessed CSI signals by simply dividing the signals from the three antenna signals with the reference signal.

Position Enhancement Algorithm: To detect breathing signal accurately in interference scenarios, it is necessary to qualitatively enhance the breathing signal in the case that walking and breathing signal mixes irregularly. According to the linear projection rules, the optimal projection interval of CSI signals under different subcarriers is obtained with known human

position information, and then the initial angle is traversed in the space of $0 \sim 180^\circ$ to obtain multiple candidate systems. The projection is performed under these different systems to filter out the group of projection angles with the largest sum of BNR values in the projected waveforms. According to Section III-C, only the respiratory signal satisfies the optimal projection rule, so the algorithm maximizes the periodic characteristics of respiratory signal, which is equivalent to achieving the enhancement of the respiratory signal in mixed signal.

Short-Time Window Shift: Due to the significant difference in walking and breathing signal, we use short time window shift to achieve a secondary enhancement of breath. This section consists of three main stages: 1) the complete CSI signal is segmented into multiple small segments by determining the appropriate transform window length; 2) a short projection transformation and strong filtering are applied to each segment using cyclic operation to suppress noise; 3) finally, multiple small segments are spliced to obtain the complete waveform, which achieves the purpose of directly suppressing noise and indirectly enhancing respiration. The waveform is superimposed with the waveform processed by the position enhancement algorithm to obtain the secondary enhancement waveform.

Multiantenna Selective Fusion Algorithm: After completing the above operations, three spatial enhancement waveforms will be obtained. However, due to the different spatial distributions of the three antennas and the phase π blurring problem brought by the optimal projection, we need to identify and correct the inverted enhancement waveforms so that the initial phases of the three waveforms are aligned. Here, we use a new metric - PAR*BNR to identify the inverted antennas and filter out the best enhanced combination waveform, where both PAR and BNR reflect the good quality of the respiratory signal, with PAR focusing on whether the respiratory component of the signal is evident or not, and BNR focusing on describing how the signal is affected by interference. Finally, respiration rate is estimated by combining those better quality antennas to calculate autocorrelation. This method can alter the spectral structure, thus obtain a spectrogram that highlights the energy of the respiratory spectrum units.

V. SYSTEM DESIGN

The specific system design for this section is shown in Fig. 7. Four components will be specified in this part: 1) data preprocessing; 2) position enhancement algorithm; 3) short time window shift; and 4) multiantenna selective fusion algorithm.

A. Data Preprocessing

The CSI signal received by the system is 3-D data in time, space, and frequency dimensions, respectively. Due to the existence of a general packet loss phenomenon of the wireless link in the process of transmitting and receiving, the actual received data is less than the expected number of time points. Therefore, in the data preprocessing link, in addition to synthesizing the equivalent signal to complete the antenna ratio, the data points are supplemented into 6000 points according to cubic spline interpolation, which facilitates the estimation of the respiration rate at a later stage.

1) *Reference Signal Synthesis*: However, due to the inherent defects of Wi-Fi hardware devices and the temporal asynchrony of transceivers, additional random phase noise, such as CFO, SFO, PDD, etc., is usually introduced to the signal, so these random phase offsets need to be removed. According to the CSI Ratio model proposed in Farsense [38], we can see that antennas from the same receiver often share the same oscillator, so a simple division of signals between the antennas can remove the random phase offset. However, since there are 6 combinations of different divisions, we need an effective screening algorithm to get the optimal antenna ratio to minimize the division distortion of the signal. Take antenna 2/1 as an example

$$\left\{ \begin{array}{l} \frac{H_2(f,t)}{H_1(f,t)} = \frac{H_{s,2}(f) + H_{d,2}(f,t) + \varepsilon_2(f,t)}{H_{s,1}(f) + H_{d,1}(f,t) + \varepsilon_1(f,t)} \\ H_{d,2}(f,t) = a_{d_t,2}(f,t)e^{-j2\pi f \frac{d_{t,2}(t)}{c}} + a_{d_i,2}(f,t)e^{-j2\pi f \frac{d_{i,2}(t)}{c}} \\ H_{d,1}(f,t) = a_{d_t,1}(f,t)e^{-j2\pi f \frac{d_{t,1}(t)}{c}} + a_{d_i,1}(f,t)e^{-j2\pi f \frac{d_{i,1}(t)}{c}} \end{array} \right. \quad (6)$$

Simple division can easily turn a signal into distortion, and although the Farsense [38] states that division does not change the shape or direction of change of the signal, this still affects the degree of signal change. Considering using all the received antenna signals to synthesize a reference signal with a small dynamic component as the denominator, the degree of signal distortion can be greatly reduced. The equivalent signal is generated as follows:

$$H_{ref} = W * H = w_1 * H_1 + w_2 * H_2 + w_3 * H_3 \quad (7)$$

where W denotes the weight matrix, H denotes the antenna signal matrix, and w_1 , w_2 , and w_3 denote the weight values of the three antennas, respectively, which is the set of weight values that minimizes the dynamic fluctuation of the generated reference signal H_{ref} . The objective of generating the reference signal is to make the reference signal minimally variable, i.e., to optimize the following objective function: $\arg \min \{\text{std}(H_{ref}) - 0\}$.

2) *CSI Ratio to Remove Random Noise*: After generating the reference signal, the simple antenna ratio is replaced by the following ratio:

$$\begin{aligned} \frac{H_2(f,t)}{H_{ref}(f,t)} &= \frac{H_{s,2}(f) + H_{d,2}(f,t) + \varepsilon_2(f,t)}{H_{s,\text{ref}}(f) + \varepsilon_{\text{ref}}(f,t)} \\ &\approx \frac{H_{s,2}(f) + H_{d,2}(f,t) + \varepsilon_2(f,t)}{H_{s,\text{ref}}(f)} \end{aligned} \quad (8)$$

where $H_2(f,t)$ denotes the CSI signal received by antenna 2 and $H_{ref}(f,t)$ denotes the reference signal obtained in the previous step, and $\varepsilon_{\text{ref}}(f,t)$ denotes the noise component of the reference signal obtained after the equivalent signal analysis, which is the combination of each noise component of the original antenna. The equation can be approximately equal to the following equation since the value of $\varepsilon_{\text{ref}}(f,t)$ is small and can be neglected compared to the static signal $H_{s,\text{ref}}(f,t)$.

At this time, the signal obtained not only directly removes the random phase noise, but also maximizes the retention of the original antenna signal fluctuations in the characteristics of the antenna. Ensure that after the antenna ratio, the breathing signal to meet the linear law of change has not been destroyed, to facilitate the subsequent processing.

B. Position Enhancement Algorithm

The position enhancement algorithm consists of two main parts: 1) the RPL-based position enhancement and 2) the spatial traversal algorithm. Among them, the spatial traversal algorithm is based on the former, which determines the optimal projection angle variation interval with a fixed slope based on the position, and then traverses the space to search for the optimal projection angles that match the initial projection angle coincidence.

1) *RPL-Based Optimal Projection Interval*: According to the Farsense [38], the CSI signals under different subcarriers correspond to an optimal projection waveform in the complex plane, and the optimal projection angle corresponding to this waveform reflects the optimal spatial resolution under the current subcarrier, i.e., the coordinate axes that can maximally present the characteristics of the respiratory cyclic changes, and if we want to enhance respiratory signals in mixed signals, we need to resolve the signals in the optimal projection space, which maximizes the characteristics of the breathing signal and randomizes the walking signal, for which we inversely use the linear projection rule for the design of the position enhancement algorithm.

The commercial Wi-Fi equipment used in this system adopts frequency domain diversity technology, the best projection angle of the signal under this frequency domain diversity under different subcarriers satisfies the linear change rule, and the fitting of curves to these best projection angles can obtain a straight line whose slope reflects the length of the RPL. Equation (9) shows the formula satisfied by the linear law of change, i.e., the slope of the optimal projection angle curves reflects the time Difference of Flight (TDOf) between dynamic and static signals. The relations satisfied by the linear projection rule are as follows:

$$\Phi' = 2\pi \Delta f (\tau_d - \tau_s) \quad (9)$$

where τ_d and τ_s denote the ToF corresponding to the dynamic and direct paths, respectively, Δf denotes the frequency interval of neighboring subcarriers, and the value of Φ' reflects the magnitude of the slope, i.e., the length of the dynamic RPL.

As shown in Fig. 8, the optimal spatial resolution of the respiratory signal is obtained by projecting the signal under each subcarrier based on this optimal projection system.

In this system, a spatial projection lineage with known optimal projection angle interval is obtained based on the known position of the human body in the experimental setup. Then the initial phase is screened by the following spatial traversal algorithm.

2) *Space Traversal Algorithm*: Under the condition that the optimal projection angle interval is known, screening is carried out in the space of $0 \sim 360^\circ$ in the step of 5° to obtain the optimal projection system under each step, and then the projected waveforms under different projection systems are calculated separately, and fast Fourier transform (FFT) are carried out sequentially to obtain the spatial spectrogram under each projection, and the waveforms in the current space are estimated by calculating the BNR value of each waveform, and a set of the best spatial projection system under which the BNR value is largest is obtained to determine the initial phase. The group with the largest BNR value is obtained to determine the optimal spatial projection system for the initial phase, which is the spatial projection system that can satisfy the maximization of the eigenvalues of the respiratory signal. This is because only when the target projection space matches the current position space, the respiratory component in the mixed signal can be maximally highlighted to achieve the purpose of respiratory enhancement.

C. Short Time Window Shift Method

After the positional enhancement algorithm, a primary enhancement waveform is obtained, and although the breathing signal has been maximally characteristically amplified, the walking signal has not been weakened either, and is still mixed in the signal. For this reason, we use the method of short time window shift to indirectly enhance the breathing signal through direct noise suppression, and superimpose it with the previous sequential enhancement waveforms to achieve the suppression of walking noise based on the enhancement of breathing, which is equivalent to the enhancement of the breathing signal twice, and the obtained waveforms are closer to the pure breathing results. This part is specifically divided into two parts: 1) the short-time segment projection enhancement filter suppression part and 2) the time multiple segment stitching part. It is divided into two parts: 1) the short-time clip projection with strong filtering and 2) the time multisegment stitching part.

Short-Time Clip Projection With Strong Filtering Due to the rapid changeability and irregularity of the walking signal, it makes it difficult to separate the breathing signal when processing the mixed signal over a long period, and even though the breathing signal is strengthened by using the positional enhancement algorithm, the interference of the walking signal

still cannot be ignored in a long period, so it is also necessary to inhibit the walking interference in the mixed signal by the method of the short-time window transform, to indirectly achieve the enhancement of the breathing signal and obtain the secondary enhancement waveform. In this part, the first step is to time stamp the lost packets according to the cubic spline interpolation to the number of packets sent during the experimental setup, and then the position-matching projection is performed according to the overall waveform to obtain the projection angle of the respiratory feature maximization and recorded and then operated on the projection angle during the subsequent short-window transform and filtering operation.

Timestamp Completion The specified number of packets set in the experiment is usually lost during the sending and receiving process. If the operation of making up for it is not carried out, the data points analyzed are fewer than the real number of points, resulting in a shorter time, and a larger error will be generated in the final analysis of the respiration rate. After making up, the calculated respiration rate is closer to the actual value.

Position-Enhanced Projections The position enhancement algorithm is processed according to the known position and a set of optimal projection angles in which the maximization of the respiratory features is achieved is recorded, and then the CSI data of each small segment is filtered based on this projection angle. The whole CSI signal is split into multiple small segments by choosing a suitable transform window length, and noise suppression is applied to each small segment. The principle of window length selection is to make the respiratory signal in the segment of data flat and approximate to a small arc, while the walking signal changes drastically with multiple peaks and troughs. In this way, the intensity of S-G filtering and smoothing filtering can be increased during the strong filtering process of this part of the data, so that the walking signal is filtered out and the trend of the respiratory signal is retained.

Time Multisegment Stitching After processing the data in small segments in a round-robin fashion, the segments are stitched together to obtain complete secondary-enhanced data. Due to the overlap of small segments between different segments during the cyclic processing, there is also overlap during stitching. The total number of data points in the experiment is 6000 points, and the number of points for each small segment is 3 times the number of sampling points, i.e., 300 points, and the number of points between two neighboring windows is 50, and the overlap rate is 1/6.

D. Multiantenna Selective Fusion Algorithm

This part consists of two aspects: 1) we evaluate the spectrum quality by combining the unique PAR and BNR metrics, and then filter out the better quality antennas by combining the soft thresholds, and then get the estimated respiration rate after fusion and 2) the waveforms of the three antennas after enhancement may have an antenna inverted, so we detect the inverted waveforms by the simple and effective sequential inverted detection method. We detect the inverted antenna by a simple and effective sequential inversion

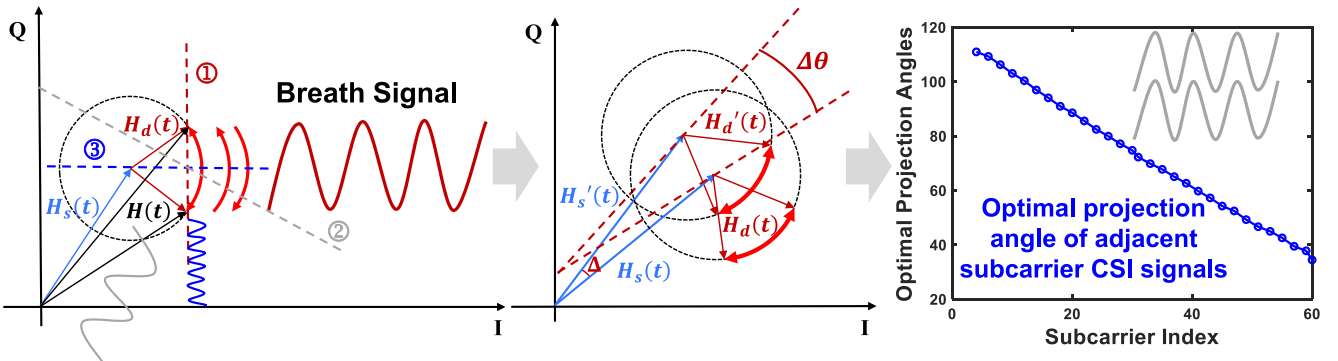


Fig. 8. Best projection degrees: The optimal projection under different subcarriers satisfies the rule of linear variation.

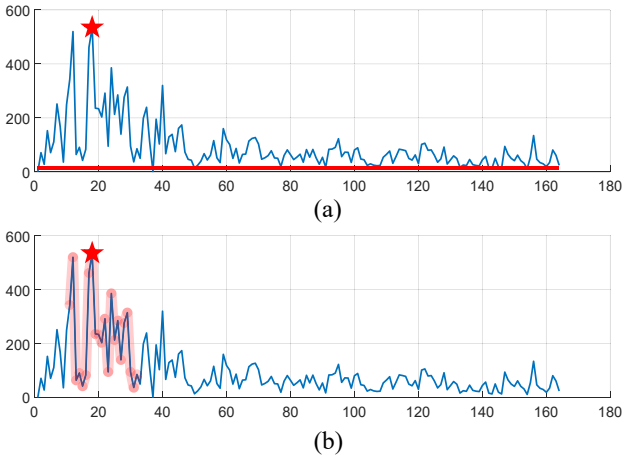


Fig. 9. Spectral representations of PAR and BNR. (a) PAR. (b) BNR.

detection method and use the corrected combined waveform as the final respiration waveform.

1) Soft Threshold Fusion Multiantenna: Due to the different spatial distribution of different antennas, the diversity signal will have a certain phase deviation when it reaches different antennas, and this stable phase deviation reflects the arrival angle of the signal, due to the different energies of different antennas, the quality of the received signals is also uneven. To get the best respiration rate estimation, we use a new type of indicator - PAR*BNR, to screen out the antennas with the larger ones for this indicator, and we find that if we only use this indicator to screen the best antennas to estimate the human respiration rate, it is easy to lose the antennas with good quality, and although the difference between the two indicators is close, the difference in the respiration rate estimation is also large, if we consider the two antennas together, and average the human respiration rate of each antenna, then we can get a more accurate respiration rate. For screening the better quality antennas we use the soft threshold method, i.e., we screen out the antennas whose metrics are greater than 0.9 times the maximum value of PAR*BNR, and then calculate the mean autocorrelation result as the final result.

PAR Indicator: an indicator used to measure the relationship between the peak value and the average value of a signal. The peak amplitude refers to the maximum amplitude value in the

signal, while the average amplitude refers to the average value of the signal amplitude., as shown in the Fig. 9(a). The value of PAR tells us whether or not there is an instantaneous peak in the signal and the size of the dynamic range of the signal. For the respiratory signal spectrogram, since the respiratory rate corresponds to a larger range of cells with larger peaks on the spectrogram, the larger the peak indicates that the respiratory signal is stronger in energy, and the respiratory characteristics are more obvious in the group of data, the better the quality of the data, moreover, the respiratory rate can be directly calculated based on the peak of the spectrum. Because this system uses 8192-point FFT, so the whole spectrum of the change range contains all the points of the interval, when there is walking interference, the whole spectrum of the mean value is larger, at this time the PAR is smaller. A weak respiratory signal and a large interference in the spectrogram corresponds to a smaller PAR value, and a strong respiratory energy and a small interference in the spectrogram corresponds to a larger PAR value. Based on this indicator, the quality of the spectrum can be screened out.

BNR Indicator: Based on the definition in the Farsense [38], BNR is a specific metric that describes the signal-to-noise ratio of the breath signal, which reflects the percentage of the total energy of the breath signal in the spectrogram, reflecting the goodness of the waveform. It is defined as the ratio of the sum of the energy of the respiratory signal units on the spectrogram to the total unit energy of the spectrum, as shown in Fig. 9(b). Larger BNR values indicate that the signal contains more respiratory components and the signal quality is better.

*PAR*BNR Indicator:* PAR describes the energy strength of the prominent unit of the respiratory signal in the spectrogram as well as the distribution of the walking interference in the spectrogram, which is a preliminary reflection of the quality of the respiratory spectrum. BNR reflects the proportion of the energy of the respiratory signal. The combination of the two can fully reflect the quality of the current signal: the larger the value of PAR*BNR, the larger the proportion of respiratory signal in the current mixed signal, the more prominent the peak unit on the spectrogram, the waveform is closer to the pure respiratory signal, and the results obtained by using spectrum estimation and autocorrelation are closer to the ground-truth.

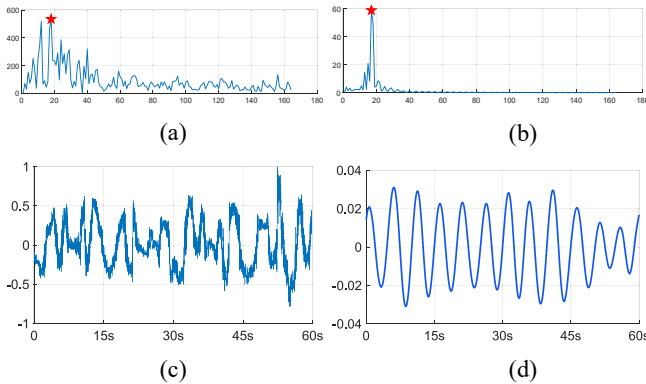


Fig. 10. Spectrograms and waveforms before and after enhancement with this system, wherein (a) and (c) denotes a respiratory spectrogram and a corresponding waveform before the use of the present system and (b) and (d) denotes a spectrogram and a waveform corresponding to the enhancement of the respiratory signal after the use of the present system.

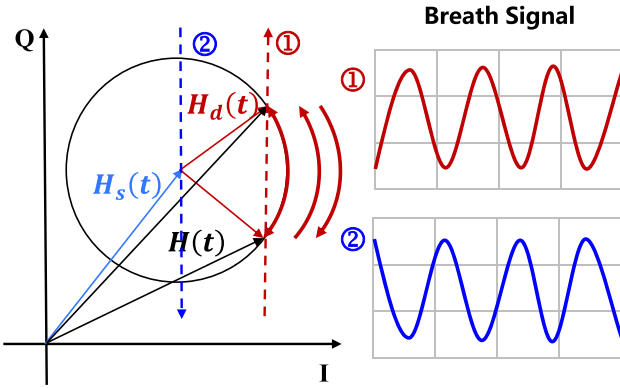


Fig. 11. Causes of π blurring during projection.

As shown in Fig. 10(b), the respiratory signal energy in the enhanced and optimally fused spectrograms is significant and close to that of the pure respiratory spectrograms, and the respiratory waveforms obtained are also more periodic, as shown in Fig. 10(d). After screening the best antennas using the above metrics, a few antennas of better quality are screened based on a soft threshold (0.9 times the maximum PAR*BNR metric). Then the average of the autocorrelation estimation of these antennas is taken as the final respiration rate estimation.

2) *π Fuzzy Detection and Correction:* Due to the unique method of enhancement, i.e., finding the projection axis with the largest projected waveform in the complex plane, which makes the waveforms obtained from the projection axes with a difference of π may have the difference of inverted phase, the reason for the inverted phase is shown in Fig. 11. Even after superimposing the waveforms of the three antennas, the waveforms obtained are similar to those of a single antenna if the π blurring is not eliminated, which does not produce a significant enhancement effect. Therefore, we adopt the algorithm of detecting the waveform of the antenna that produces inverted phase, and superimpose the waveform after correcting π blurring with the normal waveform to obtain the total waveform after combining multiple antennas, which makes the peaks and troughs of the waveform more obvious, and thus obtains the waveform that clearly reflects the respiratory fluctuation.

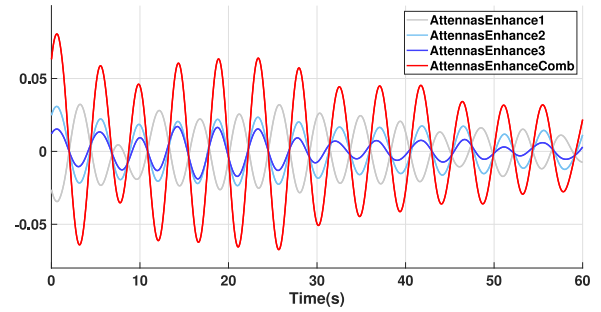


Fig. 12. Different antennas waveforms.

The specific steps of the algorithm are as follows: one of the three antennas is inverted and superimposed with the waveforms of the other two antennas, and the three antennas are directly superimposed to obtain the noninverted waveforms, the FFT of the total waveforms is calculated to obtain the PAR and BNR value, and the waveform with the largest product of the two is selected as the final breathing waveform. Combining the results, it can be found that the combined waveform with the largest result tends to correspond to the case of correcting the inverted antenna, and the resulting waveform is also the one with the most pronounced waveform and the most significant periodicity among the four candidate waveforms, as shown in Fig. 12.

VI. EXPERIMENTAL SET-UP AND EVALUATION

Experimental Deployment: We implement the *RespEnh* system using two off-the-shelf commercial Wi-Fi devices equipped with Intel 5300 network cards. We choose the device equipped with one antenna as the transmitter and the other device equipped with three antenna linear arrays as the receiver, as shown in Fig. 14(a). The distance between neighboring antennas is set to half the wavelength of Wi-Fi (2.5 cm) and a CSI tool [47] is installed in the device to collect CSI signals. The transmitter is configured to injection mode, while the receiver is set to monitor mode. The Wi-Fi signal is transmitted on channel 64, with a center frequency of 5.32 GHz and a packet transmission rate of 100 Hz within a 20 MHz bandwidth.

Experimental Setup: We implement the experiment by deploying the system in two scenarios, an open space and an indoor office. In this case, the experimental setup on controlling the precise distance to obtain parameter performance is performed in Scenario I, while Scenario II is used to explore whether the system performance can be stabilized in other scenarios (especially indoor scenarios with significant multipath effects). The experiments in Scenario I are completed by recruiting 10 volunteers, exploring the effects of breathing proximity, interference proximity, and user diversity on system performance, respectively. The ground truth respiration rate of each experiment is recorded by a commercial device (Neulog Respiration Monitor Belt logger sensor NUL236), which is connected to the PC via the accompanying Neulog USB module (USB-200), as shown in Fig. 14(b).

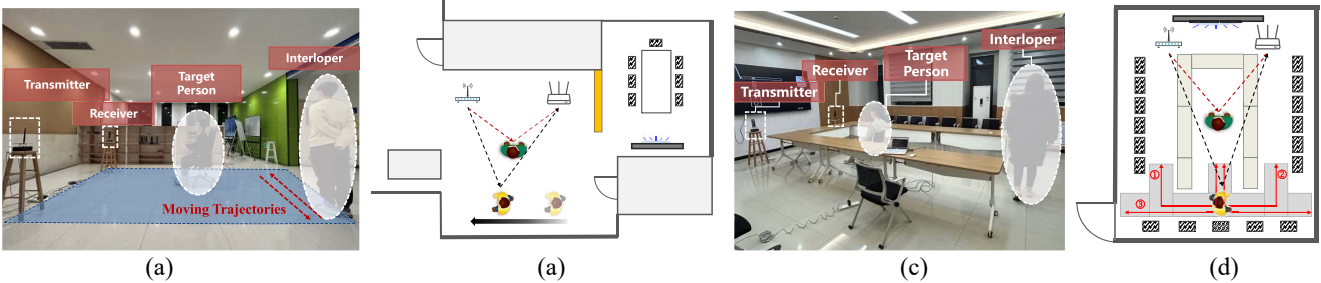


Fig. 13. Realistic scenarios and spatial floor plans of experiments. (a) Open space. (b) Plane of open space. (c) Indoor office. (d) Plane of office.

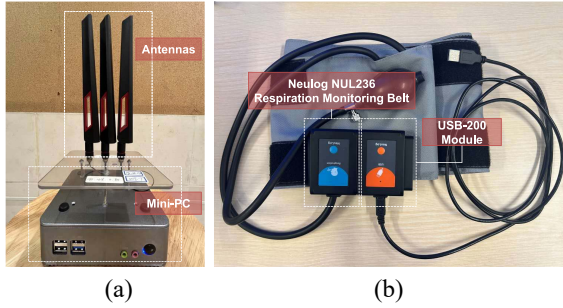


Fig. 14. Experimental equipment. (a) Tx-Rx. (b) Neulog NUL-236 respiration monitoring belt.

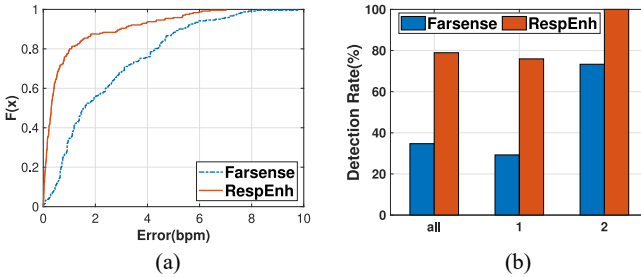


Fig. 15. Overall performance. (a) Respiration rate estimation error. (b) Detection rate.

A. Overall Performance

We conduct experiments in two scenarios: 1) an open space and 2) a conference room, with respiration rate estimation median errors of 0.81 and 0.15 bpm, respectively. The sampling rate is 100 Hz, and the respiration duration is 60 s. Compared with the existing works, this work is the first system that can work in interference scenarios, since most of the existing work is for pure breathing scenarios.

This system adds a respiratory bandpass filter to the pure respiratory Farsense algorithm as a baseline for this work, so that the Farsense system has a preliminary anti-interference performance, or else in the case where the walking interference is very close to the breathing, the system can easily fail. Fig. 15(b) shows that, compared to the reference comparison, this system can still detect the respiration rate well when the Farsense system fails, and the overall performance is improved by a factor of 2. The detection rate in this article is defined as $(N_{\text{detected}}/N_{\text{all}})$, where N_{detected} is the number of CSI measurements for which the absolute error between the

respiratory rate estimation and the ground truth is less than 1 bpm, and N_{all} is the total number of CSI measurements collected.

For some experiments containing precise distance control, we deploy our system under Scenario I and test different groups of variables, respectively, including breathers' position, unchanged while interferers' distance from near to far, interferers' position unchanged while breathers' position from near to far, different users' experiments with corresponding walking and interfering, and different duration of breath data collection. A total of 247 groups of data are collected in the experiment, each group of data collects up to 60 s, totaling 14 820 s of data. The results show that the system supports up to tolerate a relative interference distance of 2.4 m at a breathing distance of 6.4 m with a median error of 0.89 bpm.

B. Parameter Performance

Impact of Interference Distance: To demonstrate the effect of the distance of the interferer on the performance of the system, we control the distance of the respirator from the transceiver, and by calculating the error of the interferer located at different distances, we obtain the box-and-line diagram as shown in Fig. 16(a). The result proves that when the target respiratory person is kept constant, the farther away the interference distance is, the less influence it produces on the data, and the closer the obtained waveforms are to the pure respiratory scenario. The reason for analyzing this phenomenon is that the farther the walking distance is, the stronger the signal attenuation is, and the fewer components it accounts for in the received signal, the smaller the data estimation error is.

Impact of Breathing Distance: To explore the results of the system's processing of respiratory signals with interference at different distances, we explore the results produced by respiration at different distances by fixing the relative distance between walking and respiration, and then gradually moving the respirator's absolute distance. As shown in Fig. 16(b) and (c), the results show that the further away the breath is from the transceiver, the greater the error in the system's estimated respiration rate, which is because the respiration signals are weaker at greater distances, and also the interference can easily drown out the useful respiration signals.

Fig. 17 shows in detail the effect of breathing distance on the experimental effect in the case of four different volunteers. According to the result, it can be seen that due to the inherent

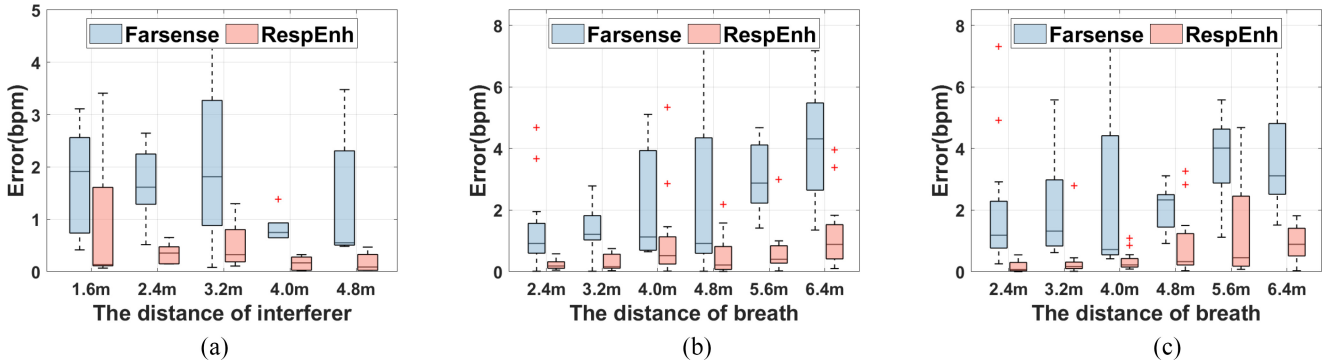


Fig. 16. Performance of the system at different breathing and interference distances, where (a) is the fixed breathing position at 2.4-m interference from near to far and (b)and (c) is the position of breathing from near to far at relative distances between interference and breathing of 2.4 and 3.2 m, respectively.

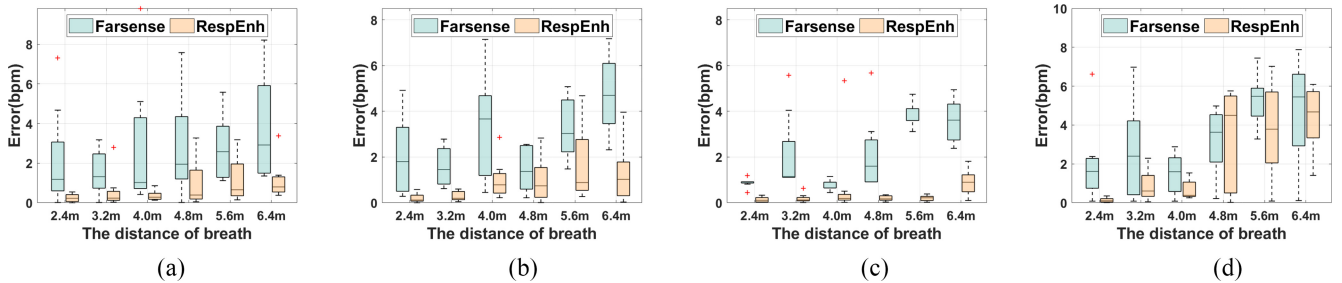


Fig. 17. Result of different person ID of same interference distance different respiratory distances, corresponding to respiratory distances from near to far, where the results of (a) Person 1, (b) Person 2, (c) Person 3, and (d) Person 4 correspond to the experimental results for each of the four different breathers.

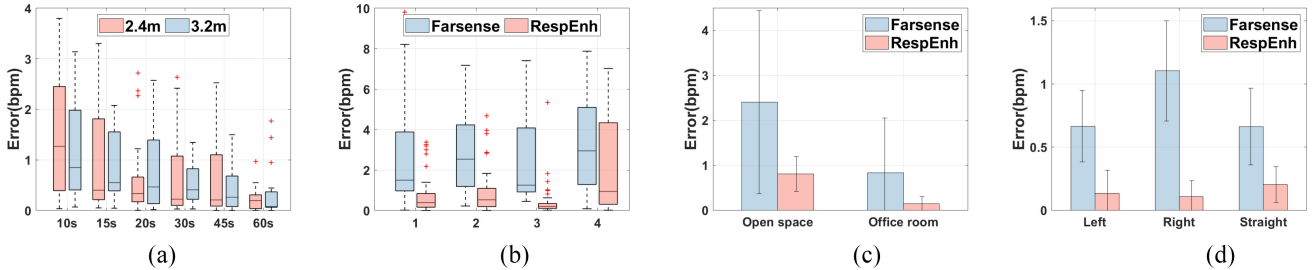


Fig. 18. Performance variation of the system under different parameter settings, where (a) denotes the error variation under different respiration times, (b) denotes the effect of user ID on the performance of the system, (c) denotes the applicability of the system in different environments, and (d) denotes the effect of different disturbance trajectories on the system.

differences in human respiration depth and rate, the results of respiration enhancement of different human beings are significantly different, but they all generally reflect the fact that the closer the respiratory distance, the better the enhancement effect is under the condition of a constant relative interference distance.

Impact of User Diversity: Different people's breathing speeds and amplitude are very different, to explore the applicability of the system to different experimenters, the system is launched in 8 volunteers, that is, four groups of breathing plus interference, and the resulting error is shown in Fig. 18(b). During the experiment, it is found that the differences in the respiration of different people are significant. However, overall, the system accuracy requirements are still met and the system achieves error rate of 0.3865, 0.5250, 0.2014, and 0.9414 bpm, respectively.

Impact of Respiration Time: The data collected for the experiment is 1 min in length each, and since the sampling rate

is 100 Hz, the number of data points contained in each piece of data is 6000. To see the minimum duration of respiration estimation that the system can support, we test the data of different durations separately and get the error line graphs as shown in Fig. 18(a). The results show that the minimum duration the system can support for the input is 20 s when the permissible error is 1 bpm, and among all the durations, the data of 60 s got the smallest error. This is because the period of respiration is large, while the time is short, such as 20 s it may contain only 3 ~ 5 respiratory cycles, if the respiration during this time is not very periodical, the error obtained by this method is larger.

Impact of the Environment: To demonstrate the effect of environmental diversity, we conduct experiments in two different scenarios: 1) an open space and 2) a conference room, as shown in Fig. 13. Fig. 18(c) shows RespEnh's respiratory rate estimation error in different scenarios. As shown in Fig. 13(c), the conference room is more crowded compared

to the open space, and obstacles, such as tables, chairs, and walls, increase the multipath effect of the signal, thus making accurate respiration estimation more challenging for the system. Nonetheless, *RespEnh* still achieves low-average respiration rate estimation errors of 0.81 and 0.15 bpm, respectively. It explains that the system works well even in indoor environments with severe multipath effects.

Impact of Different Walking Trajectories: To investigate whether there is a significant difference in the impact of walking trajectories on the system, we test the impact of three interference trajectories on the system in Scenario II. In the experiment, we, respectively, let the volunteer from the rear of the left trajectory, the right trajectory, as well as back and forth straight line walking three trajectories to interfere, and the results are shown in the Fig. 18(d), the three trajectories of the respective error are controlled within 0.137, 0.110, and 0.205 bpm. The result proves that as long as the walking position is controlled outside the anti-interference distance of the system, the trajectory does not affect the experimental results.

VII. DISCUSSION

In this work, we focus on proposing a method to enhance the respiration signal under interference scenarios, which improves the existing work with large waveform distortion and low accuracy of respiration rate estimation under interference scenarios, and becomes the most robust respiration monitoring system nowadays. However, this work still has some limitations, and there is still much room for improvement in the future. First, in anti-interference distance, this work can only control the effective perception within the interference range of 2.4 m. When the interference is closer, the effect of the system decreases.

In the future, we can explore the perception effect when the interference distance is controlled at a closer range. In addition, since breathing and walking are two different signals, we can track the walking trajectory after separating the two signals and obtain the breathing state of the stationary human body and the trajectory of the walking human body with commodity Wi-Fi in the current scene.

VIII. CONCLUSION

This article introduced *RespEnh*, a system that uses commercial Wi-Fi signals for device-free respiration monitoring to improve the condition of large errors in respiration rate estimation and severe distortion of respiration waveforms in interference scenarios. The key point of this article was to enhance the location-dependent respiratory signal using the human body location information contained in the diversity signal and also to double enhance the respiratory signal after suppressing the noise by using the short time window shift method. Finally, by comparing the enhancement results of different antennas, it was proposed to combine the enhanced antennas for a better estimation of the respiratory signal quality. The results showed that *RespEnh* can sense human respiration at a distance of up to 6.4 m, and simultaneously supports anti-interference at a relative distance of 2.4 m with

a median estimated error of 0.69 bpm, which achieved the respiration detection rate of 80% at the same time.

REFERENCES

- [1] A. D. Droitcour, "Non-contact measurement of heart and respiration rates with a single-chip microwave doppler radar," Ph.D. dissertation, Dept. Electr. Eng., Stanford Univ., Stanford, CA, USA, 2006.
- [2] C. Li, J. Ling, J. Li, and J. Lin, "Accurate Doppler radar noncontact vital sign detection using the RELAX algorithm," *IEEE Trans. Instrum. Meas.*, vol. 59, no. 3, pp. 687–695, Mar. 2010.
- [3] S. Venkatesh, C. R. Anderson, N. V. Rivera, and R. M. Buehrer, "Implementation and analysis of respiration-rate estimation using impulse-based UWB," in *Proc. IEEE Mil. Commun. Conf.*, 2005, pp. 3314–3320.
- [4] I. Immoreev and T. H. Tao, "UWB radar for patient monitoring," *IEEE Aerosp. Electron. Syst. Mag.*, vol. 23, no. 11, pp. 11–18, Nov. 2008.
- [5] F. Zhang, J. Xiong, Z. Chang, J. Ma, and D. Zhang, "Mobi²Sense: Empowering wireless sensing with mobility," in *Proc. 28th Annu. Int. Conf. Mobile Comput. Netw.*, 2022, pp. 268–281.
- [6] F. Adib, H. Mao, Z. Kabelac, D. Katabi, and R. C. Miller, "Smart homes that monitor breathing and heart rate," in *Proc. 33rd Annu. ACM Conf. Human Factors Comput. Syst.*, 2015, pp. 837–846.
- [7] Y. Hou, Y. Wang, and Y. Zheng, "TagBreathe: Monitor breathing with commodity RFID systems," in *Proc. 37th Int. Conf. Distrib. Comput. Syst. (ICDCS)*, 2017, pp. 404–413.
- [8] L. Chen et al., "LungTrack: Towards contactless and zero dead-zone respiration monitoring with commodity RFIDs," *Proc. ACM Interact., Mobile, Wearable Ubiquitous Technol.*, vol. 2, no. 3, pp. 1–22, 2019.
- [9] C. Liu, J. Xiong, L. Cai, L. Feng, X. Chen, and D. Fang, "Beyond respiration: Contactless sleep sound-activity recognition using RF signal," *Proc. ACM Interact., Mobile, Wearable Ubiquitous Technol.*, vol. 3, no. 3, pp. 1–22, 2019.
- [10] H. Abdelnasser, K. A. Harras, and M. Youssef, "UbiBreathe: A ubiquitous non-invasive WiFi-based breathing estimator," in *Proc. 16th ACM Int. Symp. Mobile Ad Hoc Netw. Comput.*, 2015, pp. 277–286.
- [11] X. Liu, J. Cao, S. Tang, and J. Wen, "Wi-Sleep: Contactless sleep monitoring via WiFi signals," in *Proc. IEEE Real-Time Syst. Symp.*, 2014, pp. 346–355.
- [12] R. Ravichandran, E. Saba, K. Y. Chen, M. Goel, S. Gupta, and S. N. Patel, "WiBreathe: Estimating respiration rate using wireless signals in natural settings in the home," in *Proc. IEEE PerCom*, 2015, pp. 131–139.
- [13] S. Yue, H. He, H. Wang, H. Rahul, and D. Katabi, "Extracting multi-person respiration from entangled RF signals," *Proc. ACM Interact., Mobile, Wearable Ubiquitous Technol.*, vol. 2, no. 2, pp. 1–22, 2018.
- [14] X. Tong, K. Liu, X. Tian, L. Fu, and X. Wang, "FineLoc: A fine-grained self-calibrating wireless indoor localization system," *IEEE Trans. Mobile Comput.*, vol. 18, no. 9, pp. 2077–2090, Sep. 2019.
- [15] X. Tong, Y. Wan, Q. Li, X. Tian, and X. Wang, "CSI fingerprinting localization with low human efforts," *IEEE/ACM Trans. Netw.*, vol. 29, no. 1, pp. 372–385, Feb. 2021.
- [16] X. Tong, H. Li, X. Tian, and X. Wang, "Wi-Fi localization enabling self-calibration," *IEEE/ACM Trans. Netw.*, vol. 29, no. 2, pp. 904–917, Apr. 2021.
- [17] X. Tong, W. Ge, Y. Tian, Z. Liu, X. Liu, and W. Qu, "NNE-tracking: A neural network enhanced framework for device-free Wi-Fi tracking," *IEEE Trans. Mobile Comput.*, early access, Jan. 29, 2024, doi: [10.1109/TMC.2024.3357569](https://doi.org/10.1109/TMC.2024.3357569).
- [18] Y. Tian, Y. Wang, Y. Tong, X. Liu, and W. Qu, "Device-free human tracking and gait recognition based on the smart speaker," *IEEE Trans. Mobile Comput.*, early access, Mar. 20, 2024, doi: [10.1109/TMC.2024.3379647](https://doi.org/10.1109/TMC.2024.3379647).
- [19] B. Xie and J. Xiong, "Combating interference for long range LoRa sensing," in *Proc. 18th Conf. Embed. Netw. Sensor Syst.*, 2020, pp. 69–81.
- [20] F. Zhang et al., "Unlocking the beamforming potential of LoRa for long-range multi-target respiration sensing," *Proc. ACM Interact., Mobile, Wearable Ubiquitous Technol.*, vol. 5, no. 2, pp. 1–25, 2021.
- [21] F. Zhang et al., "Exploring lora for long-range through-wall sensing," *Proc. ACM Interact., Mobile, Wearable Ubiquitous Technol.*, vol. 4, no. 2, pp. 1–27, 2020.
- [22] T. Wang et al., "Contactless respiration monitoring using ultrasound signal with off-the-shelf audio devices," *IEEE Internet Things J.*, vol. 6, no. 2, pp. 2959–2973, Apr. 2019.

- [23] A. Wang, J. E. Sunshine, and S. Gollakota, "Contactless infant monitoring using white noise," in *Proc. 25th Ann. Int. Conf. Mobile Comput. Netw.*, 2019, pp. 1–16.
- [24] W. Xie, R. Tian, J. Zhang, and Q. Zhang, "Noncontact respiration detection leveraging music and broadcast signals," *IEEE Internet Things J.*, vol. 8, no. 4, pp. 2931–2942, Feb. 2021.
- [25] Y. Zeng, J. Liu, J. Xiong, Z. Liu, D. Wu, and D. Zhang, "Exploring multiple antennas for long-range WiFi sensing," *Proc. ACM Interact., Mobile, Wearable Ubiquitous Technol.*, vol. 5, no. 4, pp. 1–30, 2021.
- [26] R. Paradiso, "Wearable health care system for vital signs monitoring," in *Proc. 4th Int. IEEE EMBS Special Topic Conf. Inf. Technol. Appl. Biomed.*, 2003, pp. 283–286.
- [27] B. Fang, N. D. Lane, M. Zhang, A. Boran, and F. Kawsar, "BodyScan: Enabling radio-based sensing on wearable devices for contactless activity and vital sign monitoring," in *Proc. ACM 14th Annu. Int. Conf. Mobile Syst.*, 2016, pp. 97–110.
- [28] S. Nukaya, T. Shino, Y. Kurihara, K. Watanabe, and H. Tanaka, "Noninvasive bed sensing of human biosignals via piezoceramic devices sandwiched between the floor and bed," *IEEE Sensors J.*, vol. 12, no. 3, pp. 431–438, Mar. 2012.
- [29] B. Zhai, Y. Guan, M. Catt, and T. Plötz, "Ubi-SleepNet: Advanced multimodal fusion techniques for three-stage sleep classification using ubiquitous sensing," *Proc. ACM Interact., Mobile, Wearable Ubiquitous Technol.*, vol. 5, no. 4, pp. 1–33, 2021.
- [30] N. Patwari, J. Wilson, S. Ananthanarayanan, S. K. Kasera, and D. R. Westenskow, "Monitoring breathing via signal strength in wireless networks," *IEEE Trans. Mobile Comput.*, vol. 13, no. 8, pp. 1774–1786, Aug. 2014.
- [31] O. Kaltiokallio, H. Yiğitler, R. Jäntti, and N. Patwari, "Non-invasive respiration rate monitoring using a single COTS Tx-Rx pair," in *Proc. 13th Int. Symp. Inf. Process. Sensor Netw.*, 2014, pp. 59–69.
- [32] H. Yiğitler et al., "RSS models for respiration rate monitoring," *IEEE Trans. Mobile Comput.*, vol. 19, no. 3, pp. 680–696, Mar. 2020.
- [33] X. Tian, X. Tong, and X. Wang, "RSS localization for large-scale deployment," in *Wireless Localization Techniques*. Cham, Switzerland: Springer Int. Publ., 2023, pp. 155–267.
- [34] H. Wang et al., "Human respiration detection with commodity WiFi devices: Do user location and body orientation matter?" in *Proc. ACM Int. Joint Conf. Pervasive Ubiquitous Comput.*, 2016, pp. 25–36.
- [35] X. Liu, J. Cao, S. Tang, J. Wen, and P. Guo, "Contactless respiration monitoring via off-the-shelf WiFi devices," *IEEE Trans. Mobile Comput.*, vol. 15, no. 10, pp. 2466–2479, Oct. 2016.
- [36] W. Wang, A. X. Liu, M. Shahzad, K. Ling, and S. Lu, "Understanding and modeling of WiFi signal based human activity recognition," in *Proc. 21st Annu. Int. Conf. Mobile Comput. Netw.*, 2015, pp. 65–76.
- [37] F. Zhang et al., "From Fresnel diffraction model to fine-grained human respiration sensing with commodity Wi-Fi devices," *Proc. ACM Interact., Mobile, Wearable Ubiquitous Technol.*, vol. 2, no. 1, pp. 1–23, 2018.
- [38] Y. Zeng, D. Wu, J. Xiong, E. Yi, R. Gao, and D. Zhang, "FarSense: Pushing the range limit of WiFi-based respiration sensing with CSI ratio of two antennas," in *Proc. ACM Interact., Mobile, Wearable Ubiquitous Technol.*, vol. 3, no. 3, pp. 1–26, 2019.
- [39] N. Yu, W. Wang, A. X. Liu, and L. Kong, "QGesture: Quantifying gesture distance and direction with WiFi signals," *Proc. ACM Interact., Mobile, Wearable Ubiquitous Technol.*, vol. 2, no. 1, pp. 1–23, 2018.
- [40] J. Zhu, Y. Im, S. Mishra, and S. Ha, "Calibrating time-variant, device-specific phase noise for COTS WiFi devices," in *Proc. 15th ACM Conf. Embed. Netw. Sensor Syst.*, 2017, pp. 1–12.
- [41] D. Zhang, Y. Hu, Y. Chen, and B. Zeng, "BreathTrack: Tracking indoor human breath status via commodity WiFi," *IEEE Internet Things J.*, vol. 6, no. 2, pp. 3899–3911, Apr. 2019.
- [42] Y. Zeng, D. Wu, R. Gao, T. Gu, and D. Zhang, "FullBreathe: Full human respiration detection exploiting complementarity of CSI phase and amplitude of WiFi signals," *Proc. ACM Interact., Mobile, Wearable Ubiquitous Technol.*, vol. 2, no. 3, pp. 1–19, 2018.
- [43] X. Wang et al., "Placement matters: Understanding the effects of device placement for WiFi sensing," *Proc. ACM Interact., Mobile, Wearable Ubiquitous Technol.*, vol. 6, no. 1, pp. 1–25, 2022.
- [44] Y. Li et al., "Diversense: Maximizing WiFi sensing range leveraging signal diversity," in *Proc. ACM Interact., Mobile, Wearable Ubiquitous Technol.*, vol. 6, no. 2, pp. 1–28, 2022.
- [45] X. Xie, D. Zhang, Y. Li, Y. Hu, Q. Sun, and Y. Chen, "Robust WiFi respiration sensing in the presence of interfering individual," *IEEE Trans. Mobile Comput.*, early access, Jan. 1, 2024, doi: [10.1109/TMC.2023.3348879](https://doi.org/10.1109/TMC.2023.3348879).
- [46] D. Zhang, Y. Hu, and Y. Chen, "MTrack: Tracking multiperson moving trajectories and vital signs with radio signals," *IEEE Internet Things J.*, vol. 8, no. 5, pp. 3904–3914, Mar. 2021.
- [47] D. Halperin, W. Hu, A. Sheth, and D. Wetherall, "Tool release: Gathering 802.11 n traces with channel state information," *ACM SIGCOMM Comput. Commun. Rev.*, vol. 41, no. 1, p. 53, 2011.



Jingjing Fan received the bachelor's degree from Tianjin University, Tianjin, China, in 2018, where she is currently pursuing the master's degree with the College of Intelligence and Computing.

Her research interests include wireless sensing and respiration detection.



Chenyu Pan is currently pursuing the bachelor's degree with the College of Intelligence and Computing, Tianjin University, Tianjin, China.

His research interests include wireless sensing and respiration detection.



Guanhua Zhao received the bachelor's degree from Tianjin University, Tianjin, China, in 2024 where she is currently pursuing the master's degree with the College of Intelligence and Computing.

She is currently a Senior with the College of Intelligence and Computing, Tianjin University, Tianjin, China. Her research interests include wireless sensing and respiration detection, computer version.



Xinyu Tong received the B.E. and Ph.D. degrees from the Department of Electronic Information and Electrical Engineering, Shanghai Jiao Tong University, Shanghai, China, in 2015 and 2020, respectively.

He is currently an Associate Researcher with the College of Intelligence and Computing, Tianjin University, Tianjin, China. His research papers were published in many prestigious journals and conferences, including the IEEE TRANSACTIONS ON MOBILE COMPUTING, IEEE/ACM TRANSACTIONS ON NETWORKING, MobiCom, UbiComp, and INFOCOM. His research interests include wireless sensor network and wireless localization.



Keqiu Li (Fellow, IEEE) received the bachelor's and master's degrees from the Department of Applied Mathematics, Dalian University of Technology, Dalian, China, in 1994 and 1997, respectively, and the Ph.D. degree from the Graduate School of Information Science, Japan Advanced Institute of Science and Technology, Nomi, Japan, in 2005.

He is currently a Full Professor and the Dean of the College of Intelligence and Computing, Tianjin University, Tianjin, China. He keeps working on the topics of mobile computing, datacenter, and cloud computing. He has more than 150 papers published on prestigious journals or conferences, including IEEE/ACM TRANSACTIONS ON NETWORKING, IEEE TRANSACTIONS ON PARALLEL AND DISTRIBUTED SYSTEMS, IEEE TRANSACTIONS ON COMPUTERS, IEEE TRANSACTIONS ON MOBILE COMPUTING, INFOCOM, and ICNP.

Prof. Li is the recipient of the National Science Foundation for Distinguished Young Scholars of China.



Shisheng Huang received the bachelor's degree from Communication Engineering, Department of Computer Science and Technology, Nanjing University of Posts and Telecommunications, Nanjing, China, in 2004.

He is a GM of Yangtze River Delta Anneng New Energy Technology (Shanghai) Company Ltd., Shanghai, China. He has over 20 years of working experience in Computing, Smart manufacturing and Intelligent Transportation. He used to be the Project Manager or the Technical Leader of the subject, has rich experience in science and technology project management and research and development, and has studied ten provincial major key scientific research topics. His research interests include smart manufacturing, Internet of Things, intelligent transportation, new energy digital, and big data applications.

Dr. Huang was awarded the Shanghai Science and Technology Progress Award by the Shanghai Municipal Government.